Application of a local subgrid model based on coherent structures to complex geometries

By H. Kobayashi† AND X. Wu

1. Motivation and objectives

Fine-scale coherent eddies are an important feature of turbulence. These eddies scale with the Kolmogorov microscale, and have been found universally in homogeneous isotropic turbulence, planar channel flow, and mixing layers using direct numerical simulation (Miyauchi & Tanahashi 2001). Recently, Kobayashi (2005) proposed a coherent structure model (CSM) as a subgrid scale (SGS) model. This model has been tested in a series of canonical turbulent flows including rotating and non-rotating channel flows and was found to yield a level of accuracy similar to that obtained by using the dynamic Smagorinsky model (DSM) (Germano *et al.* 1991). Compared to the DSM, the newly proposed CSM has advantages of local determination of the SGS model parameter and of faster computation. Simple and stable SGS models are suitable for engineering applications without any homogeneous directions for averaging. Since the model parameter of the CSM has a positive, finite small variance, it is stable in spite of local determination of the model parameter. This local model is suitable for complex geometries.

In this study, the applicability of the CSM is further assessed in the simulations of flow over a backward-facing step and flow in an asymmetric plane diffuser.

2. Coherent structure model

In LES, coherent structures are extracted by the second invariant Q in a resolved-scale field, which is given by

$$Q = \frac{1}{2}\left(\overline{W}_{ij}\overline{W}_{ij} - \overline{S}_{ij}\overline{S}_{ij}\right), \quad \overline{S}_{ij} = \frac{1}{2}\left(\frac{\partial \overline{u}_j}{\partial x_i} + \frac{\partial \overline{u}_i}{\partial x_j}\right), \quad \overline{W}_{ij} = \frac{1}{2}\left(\frac{\partial \overline{u}_j}{\partial x_i} - \frac{\partial \overline{u}_i}{\partial x_j}\right), \tag{2.1}$$

where $\overline{S}_{ij}$ is the strain-rate tensor, and $\overline{W}_{ij}$ is the vorticity tensor.

In the present study, the second invariant is applied to the model parameter C of the Smagorinsky model (Smagorinsky 1963):

$$\tau_{ij} = -2C\overline{\Delta}^2|\overline{S}|\overline{S}_{ij}, \quad |\overline{S}| = \sqrt{2\overline{S}_{ij}\overline{S}_{ij}}, \tag{2.2}$$

where τ_{ij} is the traceless SGS stress tensor, $\overline{\Delta}$ is the filter width, and $|\overline{S}|$ is the magnitude of the strain-rate tensor $\overline{S}_{ij}$. The model parameter C is determined as follows:

$$\begin{aligned} C &= C'\left|F_{CS}\right|^{3/2} F_\Omega, \quad F_{CS} = \frac{Q}{E}, \quad F_\Omega = 1 - F_{CS}, \\ E &= \frac{1}{2}\left(\overline{W}_{ij}\overline{W}_{ij} + \overline{S}_{ij}\overline{S}_{ij}\right), \quad C' = \frac{1}{22}, \end{aligned} \tag{2.3}$$

where F_{CS} is the coherent structure function, which is normalized by a magnitude of the

† Permanent address: Keio University, Japan

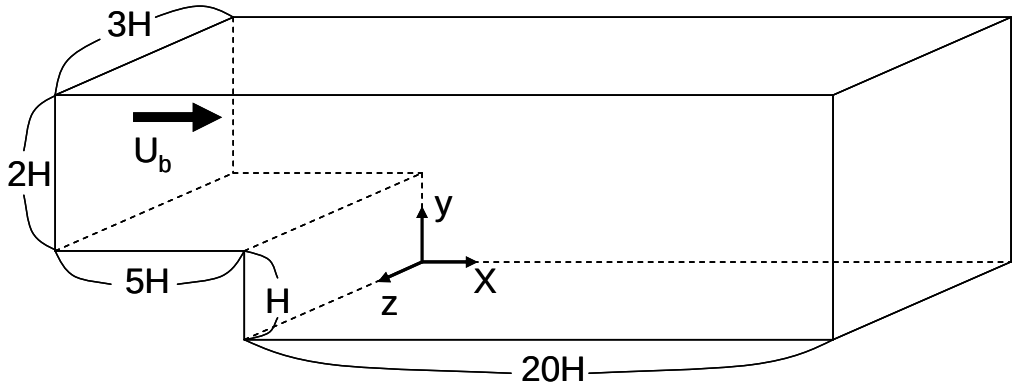

FIGURE 1. Computational domain for a backward-facing step.

shear E; F_Ω is the energy-decay suppression function. The parameter C' is determined by *a priori* tests in isotropic homogeneous and channel turbulent flows, and its value is fixed as 1/22. This model is called a coherent structure model (CSM) (Kobayashi 2005).

This model is very simple because one has only to calculate vorticities in a resolved-scale field. This model also realizes a suppression of the energy decay in a flow field with a high rotation because F_Ω gives a suppression of the dissipation with the increase in an angular velocity (Kobayashi 2005). The functions of F_{CS} and F_Ω have distinct upper and lower limits:

$$-1 \le F_{CS} \le 1, \quad 0 \le |F_{CS}| \le 1, \quad 0 \le F_\Omega \le 2. \tag{2.4}$$

As a result, the model parameter C of the CSM has a finite small variance, and the numerical simulation with the CSM is stably carried out even though the model parameter is locally determined.

The model parameter of the DSM (Germano *et al.* 1991) is determined using a least square procedure proposed by Lilly (1992) with an average in homogeneous directions.

3. Backward-facing step flow

Figure 1 shows the computational domain for a turbulent flow over a backward-facing step. The grid resolution is $256 \times 96 \times 64$ in the x, y, and z directions, respectively; x is the streamwise direction, y is the one normal to the walls, and z is the spanwise one. The Reynolds number based on the step height H and bulk velocity U_b was 4800. This value is close to 4775 in the experiment by Kasagi and Matsunaga (1995); the Reynolds number based on the step height and a centerline velocity at the inlet is 5500. The domain depth in z direction is $3H$. The grid was stretched out with the factors; 4 ($x = -5$) : 4 ($x = -1$) : 1 ($x = 0$) : 2 ($x = 2$) : 2 ($x = 10$) : 4 ($x = 20$) in the x direction; 1 ($y = 0$) : 10 ($y = 0.5$) : 1 ($y = 1$) : 20 ($y = 2$) : 1 ($y = 3$) in the y direction. An inflow condition is imposed at $x = -5$, and the inflow profile is given a fully developed channel flow at $Re_\tau = 290$. The time step is $0.01H/U_b$. A convective condition is applied at the outflow boundary. Statistics for the CSM, the DSM, and no model are accumulated over 20,000 time steps (200 time units), respectively.

This simulation was performed using JETCODE (CHUCK'S CODE), a structured incompressible flow solver developed at the Center for Turbulence Research and based on

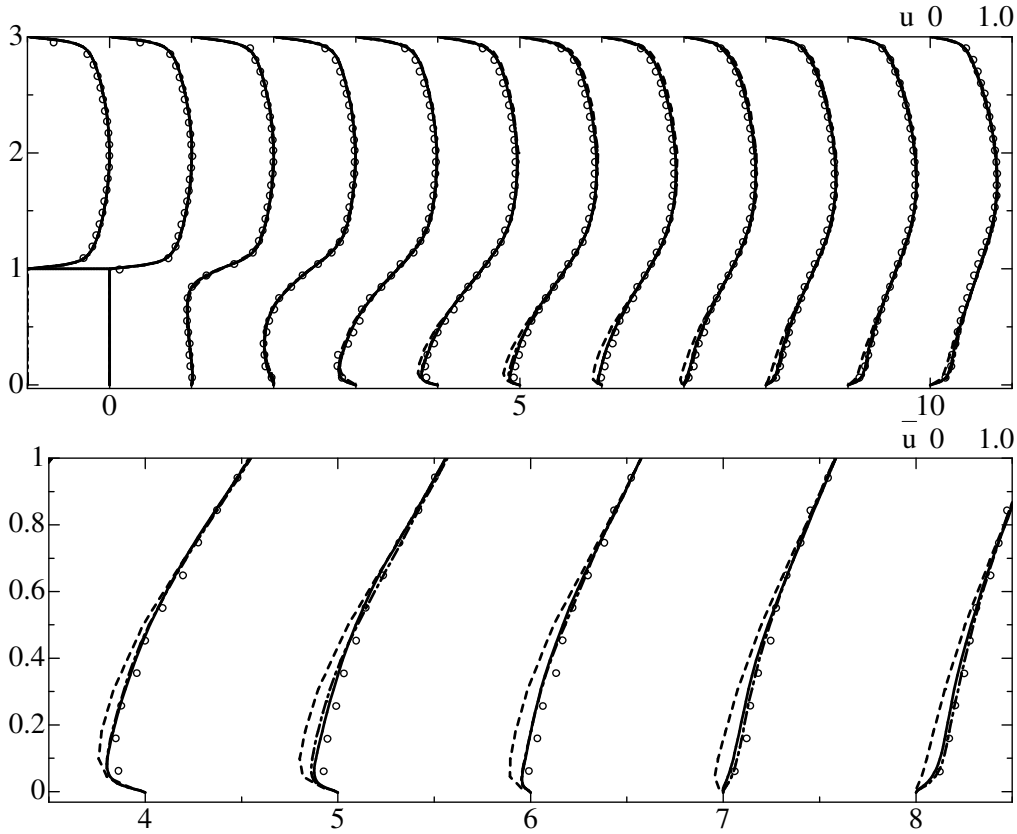

FIGURE 2. Streamwise mean velocity profiles; (upper figure): inlet $\leq x \leq 10$, $0 \leq y \leq 3$; (lower figure): $4 \leq x \leq 8$, $0 \leq y \leq 1$. ——— , CSM; —·— , DSM; - - - - , no model; ∘, experimental data by Kasagi and Matsunaga (1995).

a second-order central-discretization on a staggered-grid, a second-order time advancement, and a Poisson equation for pressure (see Akselvoll & Moin 1995; Pierce 2001).

Figure 2 shows the profiles of streamwise mean velocities for the CSM, the DSM, and no model in comparison with the particle-tracking velocimetry (PTV) data by Kasagi and Matsunaga (1995). The lower figure in Fig. 2 shows the close-up of the upper figure in a reattachment region near a lower wall. Whereas the overall profiles of the CSM, the DSM, and no model in the upper figure are almost the same, the lower figure shows that no model simulation gives under-predictions from $x = 4$ to $x = 8$ in a reattachment region near a lower wall. The CSM and DSM, however, agree well with the PTV data. The CSM gives a level of accuracy similar to the DSM in spite of a local model.

Figures 3 and 4 show the profiles of streamwise rms velocities and Reynolds shear stress for the CSM, the DSM, and no model in comparison with the PTV data by Kasagi and Matsunaga (1995). Whereas the profiles of the CSM, the DSM, and no model in Fig. 3 are almost the same, in Fig. 4 no model simulation gives under-predictions from $x = 3$ to $x = 7$ at $y = 1$ in comparison with the CSM and DSM. The profile of the CSM agrees well with that of the DSM, although the CSM is a local SGS model.

Figure 5 shows the ratios of the SGS eddy viscosity ν_t and the molecular viscosity ν for the CSM and the DSM. The ratio for the CSM becomes small at $y = 1$ because the

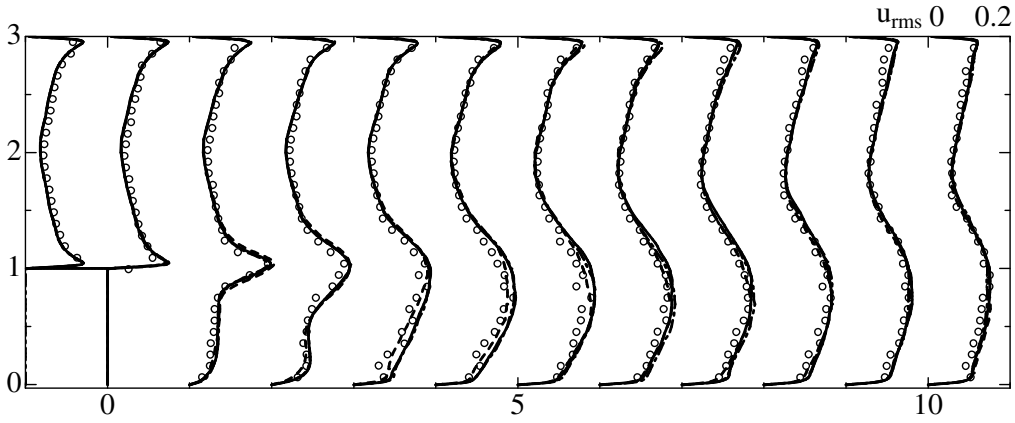

FIGURE 3. Streamwise rms velocity profiles. ——— , CSM; —·— , DSM; - - - - , no model; ∘, experimental data by Kasagi and Matsunaga (1995).

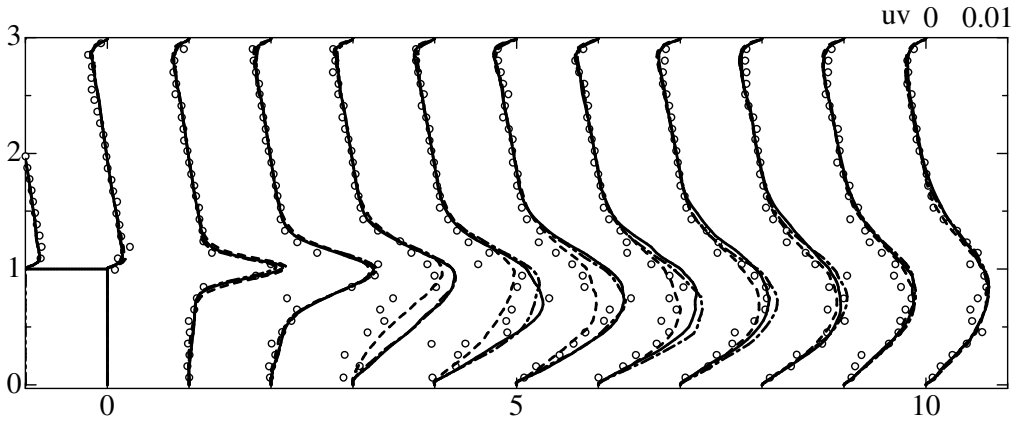

FIGURE 4. Reynolds shear stress profiles. ——— , CSM; —·— , DSM; - - - - , no model; ∘, experimental data by Kasagi and Matsunaga (1995).

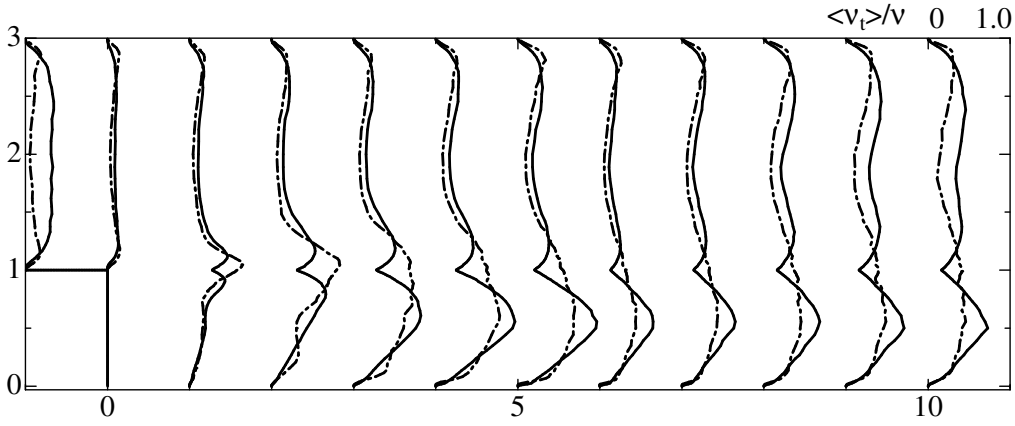

FIGURE 5. Ratios of the SGS eddy viscosity and the molecular viscosity. ——— , CSM; —·— , DSM.

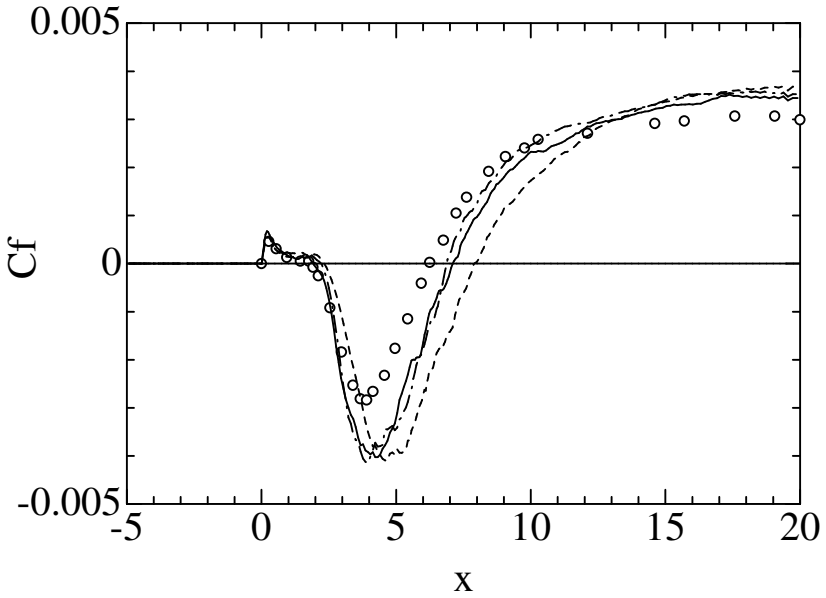

FIGURE 6. Skin friction profiles. ——— , CSM; —·— , DSM; - - - - , no model; ∘, DNS result by Le, Moin & Kim (1997).

SGS eddy viscosity depends on $\overline{\Delta}_y$ in $\overline{\Delta} = (\overline{\Delta}_x\overline{\Delta}_y\overline{\Delta}_z)^{2/3}$, and the $\overline{\Delta}_y$ is stretched out to create the finest mesh. On the other hand, in the present study the ratio for the DSM does not depend on $\overline{\Delta}_y$ because the SGS eddy viscosity is determined using an average in homogeneous directions and not using a filtering for the y direction (Germano *et al.* 1991; Lilly 1992). In the DSM the filtering in the y direction is "optional", and in some studies the filtering is carried out. In that situation the DSM would give a similar profile at $y = 1$ to the CSM.

However, the sharp profile of the CSM seems to be valid because in the small mesh the effect of ν_t to ν should be small. Although the SGS eddy viscosity of the CSM sharply changes at $y = 1$, the statistics of the first and second moments of the CSM were almost the same as those of the DSM. In addition, the CSM was numerically stable.

The CSM ran 15% faster in total CPU time than the DSM, which gives it a significant advantage over the DSM.

Figure 6 shows the skin friction profiles for the CSM, the DSM, no model, and the DNS result by Le, Moin & Kim (1997). The Reynolds number for the DNS is 5100 based on a centerline velocity and a step height. This Reynolds number is similar to 5500 in our simulation. The slight difference of the amplitude in the skin friction between the DNS and the other results comes from the difference of the expansion ratio of the backstep configuration. In our case the expansion ratio of 1.5 is used, while in the DNS that of 1.2 was used. The skin friction profiles of the CSM and DSM agree well, whereas that of no model gives a far reattachment point. The reattachment lengths for the CSM, DSM, and no model are 7.09, 6.87, and 7.88, respectively. However, an experimental result by Kasagi and Matsunaga (1995) was 6.51. A higher grid resolution of 384×192×64 with the same stretch factors as the lower one was examined to confirm the reattachment length. In that study, the reattachment lengths for the CSM, DSM, and no model are 6.81, 6.75, and 7.13, respectively. For each resolution, it is confirmed that the CSM gives a similar prediction to the DSM.

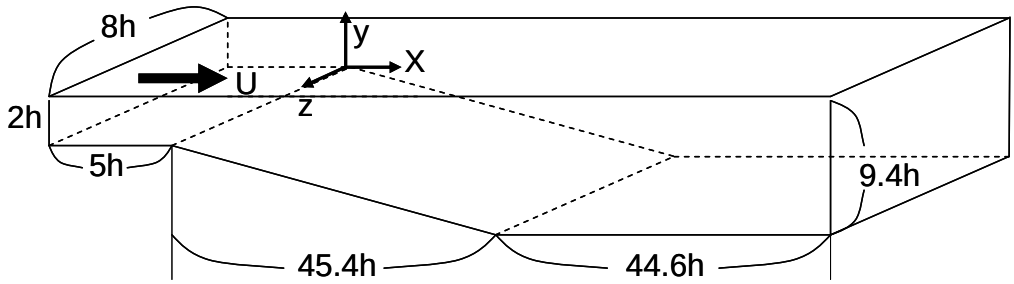

FIGURE 7. Computational domain for an asymmetric plane diffuser.

4. Diffuser flow

Figure 7 shows the computational domain for a turbulent flow through an asymmetric plane diffuser. The diffuser has a total expansion ratio of $4.7h$ and a single-sided deflection wall of 10°. An experiment for this configuration was carried out by Obi *et al.* (1993); more detailed experiments were conducted by Buice and Eaton (1997). The grid resolution is $400\times80\times80$ in the x, y, and z directions, respectively (x is the streamwise direction, y the one normal to the walls, z the spanwise one). An inflow condition is imposed at $x=-5$, and the unsteady inflow profile is given a fully developed channel flow at $Re_\tau = 500$. A convective condition is applied at the outflow boundary.

This simulation was carried out using an unstructured LES solver CDP, developed at the Center for Turbulence Research. The filtered momentum equations are solved on a cell-centered unstructured mesh with a second-order accurate central difference spatial discretization. An implicit time-advancement procedure is applied. The Poisson equation is solved to determine the pressure field. For further details about the numerical algorithm, see Ham & Iaccarino (2004); for more information about the diffuser simulation, see Wu *et al.* (2006) and Schlüter *et al.* (2005). In this study, two times larger filter width was used for the CSM.

Figure 8 shows the streamwise profiles of mean (left column) and rms (right column) velocities at $x = 5.18$, 11.96, 27.1, and 33.86 from top to bottom for the CSM, the DSM, and no model. Those figures reflect the DSM results with a finer grid resolution ($590\times100\times110$) by Wu *et al.* (2006) and the experimental data by Buice and Eaton (1997). The CSM predicts almost the same streamwise mean velocity as the fine DSM at each x location. At $x = 27.1$ the DSM and no model under-predict the mean velocity profiles at $y = 0$, while the CSM agrees with the experimental data at $y = 0$. On the other hand, the CSM gives some over-predictions near an upper wall at $x = 27.1$ and 33.86 in comparison with the DSM and no model. Overall, the streamwise mean and rms velocities of the CSM agree well with those of the fine DSM and the experiment.

Figure 9 shows the profiles of Smagorinsky constant $C_s = \sqrt{C}$ for the CSM at each x location. At the centerline of the inlet, the C_s is about 0.9. As moving downstream, the C_s increases, and at the shear layer region of $x = 33.86$ the maximum C_s gives approximately 1.4, which is close to a well-known value 1.5 in a mixing layer.

Figure 10 shows the skin friction profiles for the CSM, DSM, no model, fine DSM, and experimental data. The CSM under-predicts the skin friction from the inlet to $x = 40$ on an upper wall in comparison with the DSM and fine DSM, while the CSM gives a good prediction of the skin friction on a lower wall. Overall, the CSM predicts the skin friction similar to the DSM.

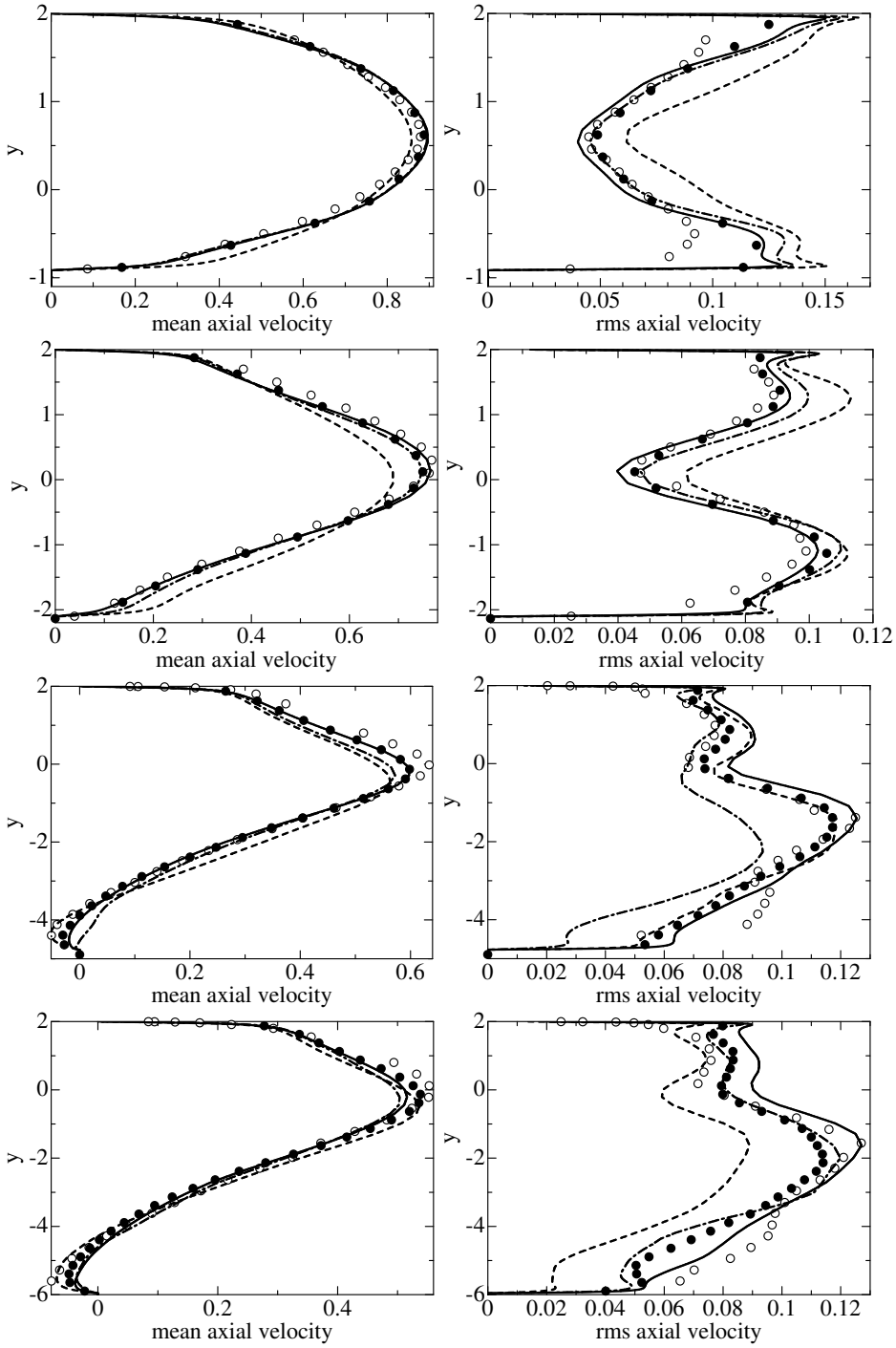

FIGURE 8. Streamwise profiles of mean (left column) and rms (right column) velocities at $x = 5.18$, 11.96, 27.1, and 33.86 from top to bottom. ——— , CSM; —·— , DSM; - - - - , no model; •, fine DSM; ○, experimental data by Buice and Eaton (1997).

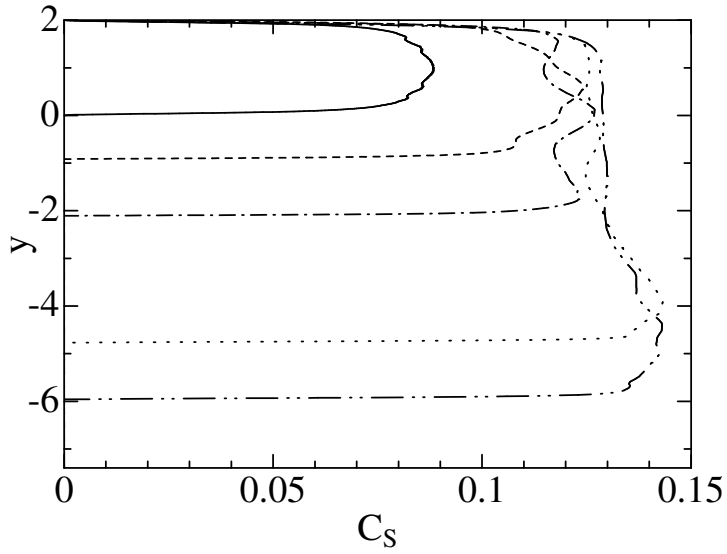

FIGURE 9. Profiles of Smagorinsky constant $C_s = \sqrt{C}$ for the CSM. ——— , $x = -5$; - - - - , 5.18; —·— , 11.96; ····· , 27.1; —··— , 33.86.

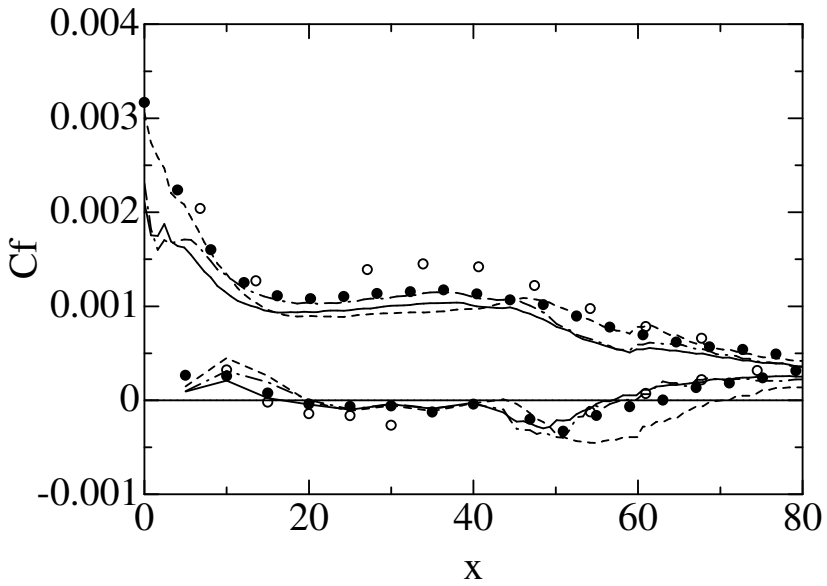

FIGURE 10. Skin friction profiles. ——— , CSM; —·— , DSM; - - - - , no model; •, fine DSM; ○, experimental data by Buice and Eaton (1997).

5. Conclusions

A local SGS model based on coherent structures has been applied to a backward-facing step flow and an asymmetric plane diffuser. A structured and an unstructured code was used for the backstep and diffuser flows, respectively. The performance of the local coherent structure model for both configurations is almost the same as the dynamic Smagorinsky model using an average in homogeneous directions. The coherent structure model is inexpensive and efficient in comparison with the dynamic model, and is nu-

merically stable without averaging. The present model will be suitable for the complex geometry without any homogeneous directions.

In the future, the local coherent structure model will be applied to a complex geometry without any homogeneous directions.

6. Acknowledgments

HK is deeply grateful to Prof. P. Moin for providing the research opportunity as a senior visiting fellow at the Center for Turbulence Research and also thanks Dr. D. You for his valuable comments and for improving the presentation of this manuscript.

REFERENCES

Akselvoll, K. & Moin, P. 1995 Large eddy simulation of turbulent confined coannualar jets and turbulent flow over a backward facing step. *Rep. TF-63, Thermosciences Division, Dept. of Mech. Eng., Stanford University.*

Buice, C. U., & Eaton, J. K. 1997 Experimental investigation of flow through an asymmetric plane diffuser. *Ph.D. Thesis, Dept. of Mech. Eng., Stanford University.*

Germano, M., Piomelli, U., Moin, P., & Cabot, W. H. 1991 A dynamic subgrid-scale eddy viscosity model. *Phys. Fluids A* **3**, 1760–1765.

Ham, F. & Iaccarino, G. 2004 Energy conservation in collocated discretization schemes on unstructured meshes. In *Annual Research Briefs-2004*, pp. 3–14. Stanford, CA: Center for Turbulence Research.

Kasagi, N. & Matsunaga, A. 1995 Three-dimensional particle-tracking velocimetry measurement of turbulences statistics and energy budget in a backward-facing step flow. *Int. J. Heat and Fluid Flow* **16**, 477–485.

Kobayashi, H. 2005 The subgrid-scale models based on coherent structures for rotating homogeneous turbulence and turbulent channel flow. *Phys. Fluids* **17**, 045104.

Le, H., Moin, P., & Kim, J. 1997 Direct numerical simulation of turbulent flow over a backward-facing step. *J. Fluid Mech.* **330**, 349–374.

Lilly, D. K. 1992 A proposed modification of the germano subgrid-scale closure method. *Phys. Fluids A* **4**, 633–635.

Miyauchi, T. & Tanahashi, M. 2001 Coherent fine scale structure in turbulence. In *IUTAM Symposium on Geometry and Statistics of Turbulence, edited by T. Kambe et al.* (Kluwer, Netherlands), 67–76.

Obi, S., Aoki, K., & Masuda, S. 1993 Experimental and computational study of turbulent separating flow in an asymmetric plane diffuser. In *Ninth Symp. Turbulent Shear Flows, Kyoto, Japan August* 16–19.

Pierce, C. D. 2001 Progress-variable approach for large-eddy simulation of turbulent combustion. *Ph.D. Thesis, Dept. of Mech. Eng., Stanford University.*

Schlüter, J., Wu, X., & Pitsch, H. 2005 Large-eddy simulation of a separated plane diffuser. *AIAA paper*, (AIAA 2005-0672), January 2005.

Smagorinsky, J. 1963 General circulation experiments with the primitive equations. I. The basic experiment. *Mon. Weather Rev.* **91**, 99–152.

Wu, X., Schlüter, J., Moin, P., Pitsch, H., Iaccarino, G., & Ham, F. 2006 Computational study on the internal layer in a diffuser. *J. Fluid Mech.* **550**, 391–412.